Time-of-Flight-Secondary Ion Mass Spectrometry and Principal Component Analysis: Determination of Structures of Lamellar Surfaces

ARTICLE *in* ANALYTICAL CHEMISTRY · MARCH 2010

Impact Factor: 5.64 · DOI: 10.1021/ac902280h · Source: PubMed

4 AUTHORS, INCLUDING:

Yiu-Ting Richard Lau
Nano and Advanced Materials Institute
19 PUBLICATIONS **87** CITATIONS
SEE PROFILE

L.T. Weng
The Hong Kong University of Science and T…
114 PUBLICATIONS **2,356** CITATIONS
SEE PROFILE

Chi-Ming Chan
The Hong Kong University of Science and T…
110 PUBLICATIONS **2,640** CITATIONS
SEE PROFILE

Anal. Chem. **2010,** *82,* 2661–2667

Time-of-Flight-Secondary Ion Mass Spectrometry and Principal Component Analysis: Determination of Structures of Lamellar Surfaces

Yiu-Ting R. Lau,[†] Lu-Tao Weng,[‡] Kai-Mo Ng,[†,§] and Chi-Ming Chan*[,†,||]

Department of Chemical and Biomolecular Engineering, Materials Characterization and Preparation Facility, Advanced Engineering Materials Facility, and Division of Environment, Hong Kong University of Science and Technology, Clear Water Bay, Hong Kong

In this article, we addressed the applicability of time-of-flight secondary ion mass spectrometry (TOF-SIMS) to examine the effects of molecular weight and of flexible-segment length on the polymer chain arrangement at the folding surfaces of the lamellae. Poly(bisphenol A−etheralkane) (C*n*) contains both rigid aromatic and flexible aliphatic CH_2 segments. The number of CH_2 units per flexible segment, *n*, varies from 8 to 12. Principal component analysis (PCA) of TOF-SIMS data revealed the chemical and structural variations of the folding surfaces of these polymers and identified the ion peaks contributing to these variations. We highlighted the discriminating power of PCA to distinguish the structural conformations of the amorphous and flat-on lamellar surfaces of these polymers. PCA loadings analyses showed that relatively more flexible structures were deposited on the folding surfaces when the flexible-segment length increased from 8 to 10 CH_2 units. The concentration of short loops at folding surfaces and the disorder of folding surfaces increased when the molecular weight increased. All these results led us to conclude that TOF-SIMS has great potential for probing the chemical composition of the folding surfaces of polymers.

Chain folding of lamellae of semicrystalline polymers was originally inferred from the interpretation of electron microscopic observations and electron diffraction of solution-grown single crystals of polyethylenes.[1] Yet these data did not reveal the important details of the molecular structures of the folding surfaces.[2] The fold models proposed to describe the chain structure at the folding surfaces were derived from indirect evidence, including spectroscopic conformation measurements as well as bulk properties, such as density, crystallinity, and heat of fusion.[2–7] In addition, various fold structures were also proposed based on results of molecular computations.[8–10] In the 1970s, neutron scattering was utilized to investigate the chain configurations of semicrystalline polymers, but conflicting results regarding the effects of molecular weight and the crystallization conditions on the fold nature were obtained.[11,12] One of the classic controversial debates was held in Faraday Discussions between the proponents of regular[13] and disordered[14] folding surfaces. The discussion was biased by the examination of small-angle neutron scattering data, which could yield equivocal interpretations for the correlation between stem distribution and fold trajectory.[15] To date, the nature of folds is still an open question in polymer physics because of the lack of definitive experimental probes.[12]

Static time-of-flight secondary ion mass spectrometry (TOF-SIMS) is a very good choice of a direct probe of the chemical structures and compositions of homopolymers[16,17] and polymer blends.[18] Its typical depth resolution is about 1 nm,[19] and its surface sensitivity is much further enhanced when the intensities of higher-mass molecular ions are measured.[20] In our earlier studies, we used TOF-SIMS to investigate the relationship between the crystalline morphology and the surface chemical composition

* Corresponding author. Phone: +852-2358-7125. Fax: +852-2358-0054. E-mail: kecmchan@ust.hk.

[†] Department of Chemical and Biomolecular Engineering.

[‡] Materials Characterization and Preparation Facility.

[§] Advanced Engineering Materials Facility.

[||] Division of Environment.

(1) Geil, P. H. *Polymer Single Crystals*, 1st ed.; Krieger: New York, 1973.
(2) Mandelkern, L. *J. Polym. Sci., Polym. Symp.* **1975**, *50*, 457.
(3) Kawai, T. *J. Polym. Sci., Part C: Polym. Lett.* **1964**, *2*, 429.
(4) Calvert, P. *J. Macromol. Sci., Chem.* **1980**, *A14*, 201.
(5) Gorce, J. P.; Spells, S. J. *Polymer* **2002**, *43*, 2581.
(6) Grasso, G.; Titman, J. J. *Macromolecules* **2009**, *42*, 4175.
(7) Viras, K.; Kelarakis, A.; Havredaki, V.; Mai, S. M.; Ryan, A. J.; Mistry, D.; Mingvanish, W.; MacKenzie, P.; Booth, C. *J. Phys. Chem. B* **2003**, *107*, 6946.
(8) Conte, G.; D'ilario, L.; Pavel, N. V.; Giglio, E. *J. Polym. Sci., Polym. Phys. Ed.* **1979**, *17*, 753.
(9) Petraccone, V.; Allegra, G.; Corradini, P. *J. Polym. Sci., Part C: Polym. Symp.* **1972**, *38*, 419.
(10) Napolitano, R.; Pirozzi, B. *Macromol. Theory Simul.* **2001**, *10*, 532.
(11) Fischer, E. W. *Pure Appl. Chem.* **1978**, *50*, 1319.
(12) Phillips, P. J. *Rep. Prog. Phys.* **1990**, *53*, 549.
(13) Guttman, C. M.; Hoffman, J. D.; DiMarzio, E. A. *Faraday Discuss. Chem. Soc.* **1979**, *68*, 297.
(14) Yoon, D. Y.; Flory, P. J. *Faraday Discuss. Chem. Soc.* **1979**, *68*, 288.
(15) Keller, A. *Faraday Discuss. Chem. Soc.* **1979**, *68*, 145.
(16) Briggs, D.; Fletcher, I. W.; Goncalves, N. M. *Surf. Interface Anal.* **2000**, *29*, 303.
(17) Briggs, D.; Fletcher, I. W.; Goncalves, N. M. *Surf. Interface Anal.* **2002**, *33*, 178.
(18) Vanden Eynde, X.; Bertrand, P. *Surf. Interface Anal.* **1999**, *27*, 157.
(19) Grams, J. *New Trends and Potentialities of ToF-SIMS in Surface Studies*, 1st ed.; Nova Science Publishers: New York, 2007.
(20) Delcorte, A.; Bertrand, P.; Arys, X.; Jonas, A.; Wischerhoff, E.; Mayer, B.; Laschewsky, A. *Surf. Sci.* **1996**, *366*, 149.

10.1021/ac902280h
Published on Web 03/10/2010

Scheme 1

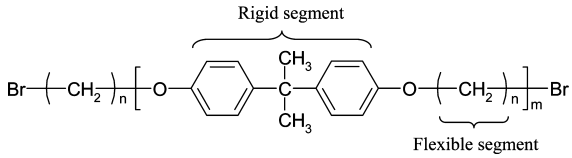

of polymers,[21−25] and our results have shown that TOF-SIMS is very sensitive to the detection of the lamellar orientations of polymers at the surfaces.[24,25] In this work, we used TOF-SIMS combined with principal component analysis (PCA) to investigate the chemical structural composition of folding surfaces of the lamellae of semiflexible polymers, poly(bisphenol A−etheralkanes) (C*n*), as a function of the molecular weight and the flexible-segment length. PCA has been performed on static SIMS spectra and chemical images of organic and biological materials.[26−32] Our results show that PCA loadings can reveal the relationship between the secondary-ion formation and the fold conformation of polymers.

EXPERIMENTAL SECTION

Poly(bisphenol A−etheroctanes) (C8), poly(bisphenol A−etherdecanes) (C10), and poly(bisphenol A−etherdodecanes) (C12) were synthesized by condensation polymerization[33] of bisphenol A with a slight excess of 1,8-dibromooctane, 1,10-dibromodecane, and 1,12-dibromododecane, respectively, to ensure that all chain ends were terminated with bromine atoms. Scheme 1 shows the general chemical structure of the repeat segment of the three polymers. Table 1 summarizes the molecular weights and the melting temperatures of the polymers, which were obtained, respectively, by gel permeation chromatography and differential scanning calorimetry. Each sample was dissolved in chloroform at a concentration of 30 mg mL^{-1}. Films of a thickness of about 100 nm were produced by spin-coating the solutions at a speed of 3 000 rpm on native silicon substrates. The polymer films were cyro-quenched to keep them staying in the amorphous state. Some of which were then annealed isothermally to equilibrium at a temperature of 80 ± 1 °C for 3 days in a ventilated oven under nitrogen purge. Lamellae with the flat-on orientation were preferentially grown on the polymer thin films at this crystallization temperature.[24] Parts a and b of

Table 1. Thermal Properties of the C*n* Polymers (*n* = 8, 10, and 12) with Various Molecular Weights

notation	M_n[a] (g mol^{-1})	PDI[b]	T_g[c] (°C)	T_m[d] (°C)
C8-1	9 100	1.58	16	88
C8-2	13 800	1.54	22	92
C8-3	16 400	1.52	24	93
C10-1	11 800	1.45	11	90
C10-2	15 700	1.47	13	91
C12-1	12 100	1.43	4	91

[a] Number-average molecular weights, measured with gel permeation chromatography. [b] Polydispersity. [c] Thermal glass transition temperatures, determined by PerkinElmer Diamond DSC at a heating rate of 10 °C min^{-1}. [d] Equilibrium melting temperatures, estimated by linear extrapolations of Hoffman−Weeks plots of the melting temperature against the crystallization temperature.

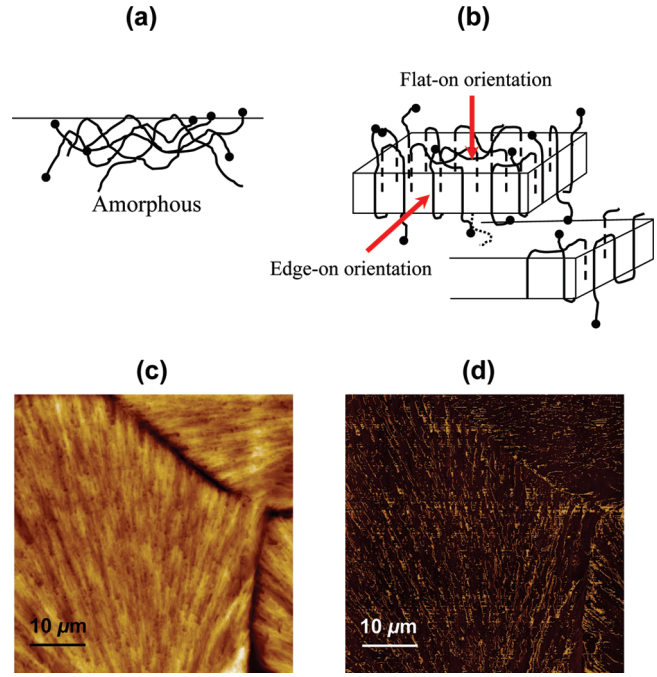

Figure 1. (a) Schematic of an amorphous surface, (b) schematic of the flat-on and edge-on orientations of a lamella, (c) typical AFM height, and (d) phase images of the surface of a 100 nm C10-1 polymer film after crystallization at 80 °C.

Figure 1 display the structural models of the amorphous surface and the flat-on lamellar surface, respectively. Parts c and d of Figure 1 are atomic force microscopic (AFM) height and phase images, respectively, showing the morphology of the flat-on lamellae of a C10-1 polymer thin film crystallized at 80 °C.

Static SIMS spectra were obtained from an Ion-ToF GmbH (Münster, Germany) TOF-SIMS V spectrometer. Bi_3^+ primary ions, which were accelerated at 25 kV and had an average pulsed current of 0.6−1.0 pA, were used to bombard fresh and annealed polymer film surfaces in the bunched mode. Three positive and three negative spectra were recorded for each specimen. The raster area was 200 μm × 200 μm. The acquisition time for each spectrum was 50 s. This resulted in an ion flux dosage of less than 3×10^{11} ions cm^{-2}, meeting static SIMS conditions. Preprocessing of the spectral data involved mass calibration and extraction of the areas of the fingerprint ion peaks with the mass-to-charge ratio (m/z) of 1 to 230 Da (with peak intensity above 100 counts) by the Ionspec

(21) Li, L.; Ng, K. M.; Chan, C. M.; Feng, J. Y.; Zeng, X. M.; Weng, L. T. *Macromolecules* **2000**, *33*, 5588.
(22) Cheung, Z. L.; Weng, L. T.; Chan, C. M.; Hou, W. M.; Li, L. *Langmuir* **2005**, *21*, 7968.
(23) Wang, Y.; Chan, C. M.; Li, L.; Ng, K. M. *Langmuir* **2006**, *22*, 7384.
(24) Lau, Y. T. R.; Weng, L. T.; Ng, K. M.; Chan, C. M. *Appl. Surf. Sci.* **2008**, *255*, 1001.
(25) Lau, Y. T. R.; Schultz, J. M.; Weng, L. T.; Ng, K. M.; Chan, C. M. *Langmuir* **2009**, *25*, 8263.
(26) Vanden Eynde, X.; Bertrand, P. *Surf. Interface Anal.* **1997**, *25*, 878.
(27) Wagner, M. S.; Tyler, B. J.; Castner, D. G. *Anal. Chem.* **2002**, *74*, 1824.
(28) Lee, J. L. S.; Gilmore, I. S.; Seah, M. P. *Surf. Interface Anal.* **2008**, *40*, 1.
(29) Biesinger, M. C.; Paepegaey, P. Y.; Mclntyre, N. S.; Harbottle, R. R.; Petersen, N. O. *Anal. Chem.* **2002**, *74*, 5711.
(30) Yang, L.; Lua, Y. Y.; Jiang, G. L.; Tyler, B. J.; Linford, M. R. *Anal. Chem.* **2005**, *77*, 4654.
(31) Tyler, B. J.; Rayal, G.; Castner, D. G. *Biomaterials* **2007**, *28*, 2412.
(32) Wagner, M. S.; Graham, D. J.; Ratner, B. D.; Castner, D. G. *Surf. Sci.* **2004**, *570*, 78.
(33) Li, L.; Chan, C. M.; Liu, S. Y.; An, L.; Ng, K. M.; Weng, L. T.; Ho, K. C. *Macromolecules* **2000**, *33*, 8002.

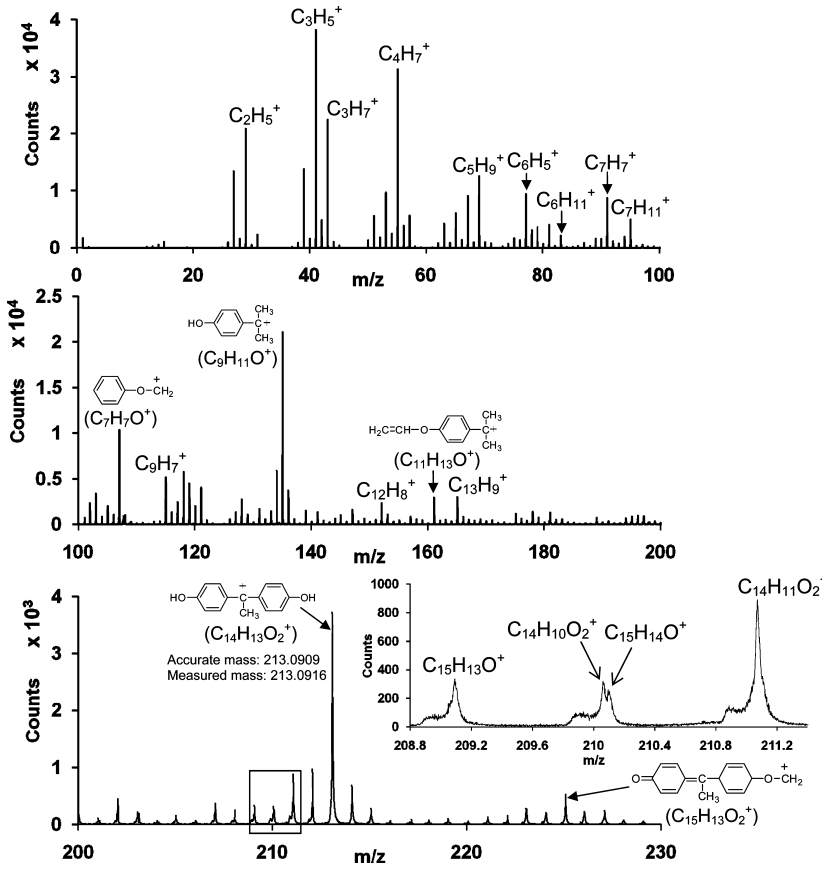

Figure 2. Positive ion spectrum of the surface of a C10-1 polymer film crystallized at 80 °C.

software. The selected mass range covered most of the fragment ions commonly obtained from the polymers listed in Table 1. Three positive masses (CH_3^+, $C_2H_3^+$, and CH_3O^+ with m/z of 15, 27, and 31, respectively) were chosen to be the calibration set for positive ion spectra. Mass calibration errors were maintained at below 10 ppm. The mass resolutions ($m/\Delta m$) of the positive ions at $m/z = 43$ ($C_3H_7^+$) and at $m/z = 107$ ($C_7H_7O^+$) were determined to be above 6 000 and above 7 000, respectively.

Figure 2 shows a typical positive ion spectrum of a C10-1 polymer crystallized at 80 °C. At the high-mass region of the spectrum, more ion peaks with the same nominal masses showed double splitting, as illustrated in Figure 2. The ion assignment was based on accurate mass determination. Typical flexible-segment positive ions, such as $C_2H_5^+$, $C_3H_5^+$, $C_3H_7^+$, $C_4H_7^+$, $C_5H_9^+$, $C_6H_{11}^+$, and $C_7H_{11}^+$ and rigid-segment ions, such as $C_6H_5^+$, $C_7H_7^+$, $C_9H_7^+$, $C_{12}H_8^+$, $C_{13}H_9^+$, $C_{11}H_{13}O^+$, $C_{14}H_{13}O_2^+$, and $C_{15}H_{13}O_2^+$, with proposed chemical structures are listed in Figure 2.

Prior to PCA, the ion peak areas were normalized to the total ion peak areas for each mass spectrum. The normalized data were then mean-centered for PCA calculations. All these operations were performed using the covariance module by the Xlstat version 2009.3.01 (Addinsoft) software. PCA reduces the dimensionality of a data set comprised of a huge number of interrelated ion variables and identifies relevant information in terms of principal components that account for much of the variability of the data set in the descending order of principal component 1 (PC1), PC2, PC3, and so forth. Two loadings plots (a standard loadings plot and a correlation loadings plot), which were generated on the mean-centered data, were analyzed to identify the one that could provide the most useful information. The correlation loadings coordinates of a given variable are the square roots of the explained variance for each principal component. Details of correlation loadings are described elsewhere.[34]

RESULTS AND DISCUSSION

Figure 3a shows a PCA scores plot of the observations based on positive ions, where the two axes are the first two PCs (PC1 and PC2). The information shown in this plot is the most representative since PC1 and PC2 account for about 91% of the total variance of the mass spectra. These polymers have different flexible-segment lengths and also different molecular weights. The amorphous and flat-on lamellar surfaces of each polymer were studied. A total of 12 discrete clustered sets of observations on the scores plots were obtained. A lucid multivariate pattern was recognized. The PC1 scores of the amorphous and flat-on lamellar surfaces of the C8 polymer were quite different from that of the C10 and C12 polymers, while the difference of the PC1 scores between the C10 and C12 polymers was much less. This result suggests a possible transition of the structural conformation when the length of the flexible segment is increased from 8 to 12 CH_2 units. The PC1 and PC2 scores of the amorphous and flat-on-lamellar surfaces allow us to differentiate between the C8 and C10 polymers with different molecular weights. The fact that we can differentiate between the amorphous and flat-on lamellar

(34) Martens, H.; Martens, M. *Multivariate Analysis of Quality: An Introduction*, 1st ed.; Wiley: Chichester, U.K., 2001.

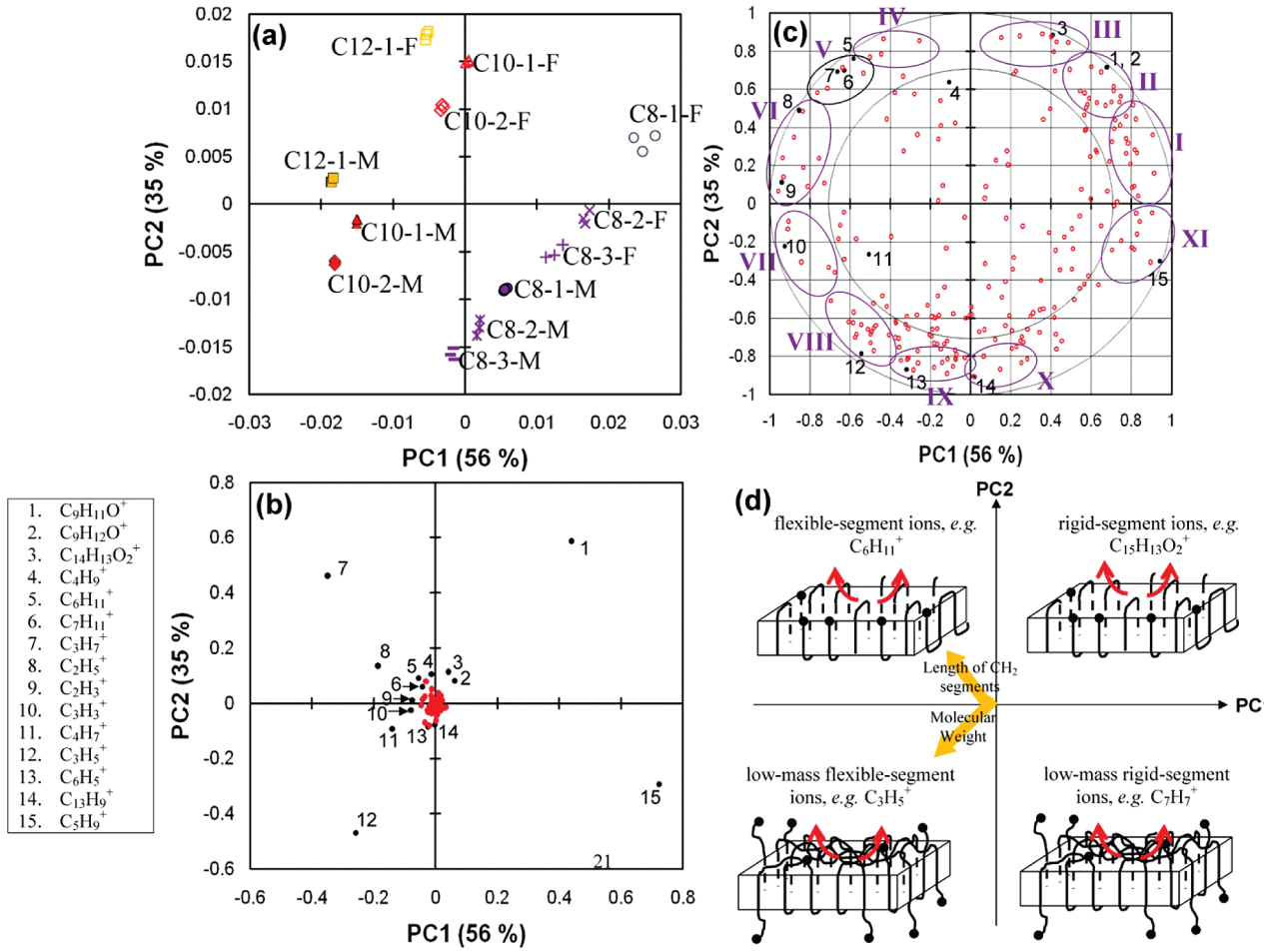

Figure 3. (a) The PCA scores plot of a total of 36 positive ion mass spectra (after normalization and mean-centering) acquired from the amorphous surface (M) and the folding surfaces (F) of flat-on lamellae of C8, C10, and C12 polymer thin films with thicknesses of 100 nm. Three spectra were acquired from each type of surface. The folding surface of the flat-on lamellae of the C8-1 polymer and the amorphous surface of the C10-2 polymer are denoted by C8-1-F and C10-2-M, respectively. The other descriptors follow the same rule. (b) Standard and (c) correlation loadings plot of positive ions (*m*/*z* 1−230 Da). The ion peaks in part c are classified into a total of 11 groups (I−XI) with the boundaries dictated by the sign and the cutoff loadings value on the PC1 and the PC2 axes. Each black dot in part c denotes a particular outlier identified on the standard plot in part b. (d) A 2-D projection of 2-fold models (regular and disordered surfaces) onto the space spanned by the first two orthogonal PC axes as a function of the flexible-segment length and the molecular weight. The fold chemical structures were deduced based on the interpretation of the scores and loadings results of positive ions.

surfaces implies that the surfaces of the flat-on lamellae did not contain a layer of highly disordered amorphous material. The C*n* polymers, which possess a longer flexible-segment length and a lower molecular weight, have more positive PC2 scores. Thus, detailed loadings analyses of individual ion peaks of the mass spectra have to be performed in order to understand how the chemical structures of the polymers are related to PC1 and PC2 scores. These PCA results indicate that TOF-SIMS can discriminate the structural conformation between the amorphous and folding surfaces.

The loading defines the size of contribution of each ion-peak variable to the PC. It is a value ranging between −1 and 1. If the score of a spectral observation and the loading of a variable on a particular PC have the same sign, the variable has a strong relationship with the observation. The larger the scores and loadings are, the stronger the relationship. Parts b and c of Figure 3 show a standard loadings plot and a correlation loadings plot, respectively. The identities of the outliers in the standard plot are listed, and their corresponding positions in the correlation loadings plot are highlighted. A standard loadings plot is constructed on the absolute numerical differences. Most often, the ion intensities are not spanned in the same numerical range. When the intensities are not scaled, the ions, which have low intensities (particularly high-mass ions), may not span a large part of the range and their strong correlations with the PC may not be revealed. A correlation loadings plot is useful in a way that it is a scale-invariant presentation of the variables, especially in cases where different numerical ranges are present.[34] Figure 3c displays the loading of each individual positive ion in a correlation circle. The squared sum of the loadings coordinates for a given ion represents the variance explained by this ion. Two circles were drawn on the plot. The outer and inner circles convey 100 and 50% of the explained variance, respectively. The ions inside the inner circle were not considered for our interpretation because these ions have weak connections with either the PC1 or PC2 axis, while the ions scattered in the annular ring were classified into 11 groups. The classification and the group boundary were determined based on the sign and the cutoff value of the loadings. For example, in the PC1(+)−PC2(+) quadrant, group I contains the ions with high positive loadings between 0.7 and 1 on PC1 but with rather small positive loadings

Table 2. Identities of Representative Ions in Groups I–XI As Shown in Figure 3c[a]

group	representative ions
I	$C_9H_9O^+$ (133), $C_{10}H_{11}O^+$ (147), $C_{12}H_{13}O^+$ (173), $C_{15}H_{13}O^+$ (209), $C_{15}H_{12}O_2^+$ (224)
II	$C_9H_{11}O^+$ (135), $C_9H_{12}O^+$ (136), $C_{10}H_{13}O^+$ (149), $C_{13}H_{13}O^+$ (185), $C_{15}H_{11}O_2^+$ (223)
III	$C_8H_9O^+$ (121), $C_{11}H_{13}O^+$ (161), $C_{14}H_{12}O_2^+$ (212), $C_{14}H_{13}O_2^+$ (213), $C_{15}H_{13}O_2^+$ (225)
IV	$C_6H_9^+$ (**81**), $C_7H_9^+$ (**93**), $C_7H_{13}^+$ (**97**)
V	$C_2H_6^+$ (**30**), $C_3H_7^+$ (**43**), $C_6H_8^+$ (**80**), $C_6H_{11}^+$ (**83**), $C_7H_{11}^+$ (**95**)
VI	$C_2H_3^+$ ($27^{\#}$), $C_2H_5^+$ (**29**), $C_3H_6^+/C_2H_2O^+$ (**42**), $C_4H_6^+$ (**54**), $C_4H_3O^+$ (**67**)
VII	$C_3H_3^+$ (**39**), $C_4H_4^+$ (**52**), $C_4H_5^+$ (**53**), C_3HO^+ ($53^{\#}$), $C_5H_6^+$ (**66**)
VIII	$C_3H_5^+$ (**41**), $C_5H_3^+$ ($63^{\#}$), $C_6H_6^+$ ($78^{\#}$), $C_9H_7^+$ (115), $C_{10}H_8^+$ (128)
IX	$C_3H_3O^+$ ($55^{\#}$), $C_6H_5^+$ (77), $C_7H_7^+$ (91), $C_8H_7^+$ ($103^{\#}$), $C_{12}H_8^+$ (152)
X	$C_8H_6^+$ ($102^{\#}$), $C_{13}H_9^+$ (165), $C_{12}H_6O^+$ (166), $C_{14}H_{10}^+$ (178), $C_{15}H_9^+$ (189)
XI	$C_5H_9^+$ (**69**), $C_5H_{10}^+$ (**70**), $C_8H_{13}^+$ (**109**), $C_{14}H_{11}O^+$ (195), $C_{14}H_{12}O^+$ (196)

[a] The number inside the parentheses is the m/z ratio (in Daltons). The ion masses in bold and without bold represent the flexible and rigid segment, respectively.The ion mass specified with a superscript "#" means that the identity may be somewhere between the flexible and the rigid segment of the polymers.

on PC2. Group II contains the ions with moderately positive loadings between 0.5 and 0.7 on both PC1 and PC2. Group III contains the ions with small positive loadings on PC1 but with large positive loadings between 0.7 and 1 on PC2. The same rule applies to the other three quadrants.

The chemical structures of representative positive ions in each group are summarized in Table 2. Ions in group I contributed most to the positive score on PC1 in the PC1(+)−PC2(+) quadrant, followed by the ions in group II and then those in group III in descending order of the magnitude of the PC1 loading. The ion structures in groups II and III are very similar to those in group I. One discernible difference between the standard (c.f., Figure 3b) and the correlation loadings plots (cf., Figure 3c) is that many high-mass ion fragments, which were supplanted in the standard loadings plot, were revealed. These ions, which are basically in the form of $C_iH_jO^+$ and $C_iH_jO_2^+$, are highly unsaturated. They were uniquely fragmentized from the rigid segments of the Cn polymers. For example, the highest-m/z ion, $C_{15}H_{12}O_2^+$ ($m/z = 224$), in group I is a nearly intact bisphenol A unit cation. This result suggests that there is a larger tendency for the deposition of the rigid segments on the surfaces of the Cn polymers when the PC1 score becomes more positive. C8-1-F, which denotes the folding surface of the lamellae of the C8-1 polymer and is located in the PC1(+)−PC2(+) quadrant, has the highest positive score on PC1. Hence, we can conclude that the surface of this polymer had a high concentration of rigid segments, suggesting that the folding surface consisted largely of the bisphenol A units. On the contrary, the folding surfaces of the C10 and C12 polymers, such as C10-2-F and C12-1-F, which are located in the upper left PC1(−)−PC2(+) quadrant, were the sources of the hydrocarbon ions, ($C_iH_j^+$), with a moderate to high degree of saturation. The $C_iH_j^+$ ions of C10-2-F and C12-1-F are located in groups IV and V, respectively. These ions, such as the $C_7H_{13}^+$ ion in group IV and $C_6H_{11}^+$ ion in group V, are exemplary of the flexible segments of the polymers. The sign and the magnitude of the score of PC1 can be used to determine the nature of the folds of the Cn polymers.

Given the same sign and the same magnitude of the PC1 score, it is apparent that the PC2 axis is related to the degree of order of the folding surfaces of the polymers. This conclusion was deduced based on the interpretation of the molecular weight effect on the folding surfaces from the PCA results. On the basis of the fact that both the PC1 and PC2 scores of the amorphous and folding surfaces consistently shifted to more positive values when the molecular weight of the Cn polymers decreased, we can conclude that the surface concentration of the rigid segments of the C8 and C10 polymers increased as the molecular weight of the polymers decreased. The surface structural transition pertaining to the score change with molecular weight can be determined by comparing the characteristics of the contributing ions in groups I and XI. It is important to note that these two groups of ions have positive PC1 loadings but opposite signs of PC2 loadings. The ions in group XI were ascribed to the folding surfaces, denoted by C8-2-F and C8-3-F, which had positive loadings on PC1 but small negative loadings on PC2 in the PC1(+)−PC2(−) quadrant. Apart from the $C_iH_jO^+$ ions, which are indicative of the rigid segments, other ions with a higher degree of saturation, such as $C_5H_9^+$, $C_5H_{10}^+$, and $C_8H_{13}^+$, are present in group XI (cf., Table 2). These highly saturated ions are characteristic of the flexible segments of the Cn polymers. The existence of short loops of uncrystallized stems on the folding surfaces of the C8-2 and C8-3 polymers, which have higher molecular weights than the C8-1 polymer, was responsible for the appearance of both rigid- and flexible-segment ions. As shown in Figure 3a, the folding surface of the C8-3 polymer, designated by C8-3-F, is located near the amorphous surface of the C8-1 polymer, designated by C8-1-M. Therefore, if a polymer with a molecular weight higher than that of the C8-3 polymer was used in this analysis, the folding surface of this polymer would have been predicted to contain a disordered layer resembling that of the C8-1-M. This is an obvious outcome of molecular mass fractionation, whereby the lower-molecular-weight components are inclined to be excluded from the bulk and remain on the surface of the flat-on lamellae.[23] In short, we have offered direct evidence through the use of TOF-SIMS that the chemical structural regularity of the folding surfaces decreases with the molecular weight of the polymers as one would expect. This is because high-molecular weight polymers were susceptible to the curbs on the selectivity of the fold structures during crystallization as a consequence of kinetic constraints to overcome the torsions and deformations of a longer slice of polymer chains at the growth front of the lamellae. The PC2 axis governs the potentiality of having a regular or random folding surface of the polymers. A more negative PC2 score is appertaining to a decrease in the regularity of the surface structures. Thus, the folding surface of a polymer with a larger

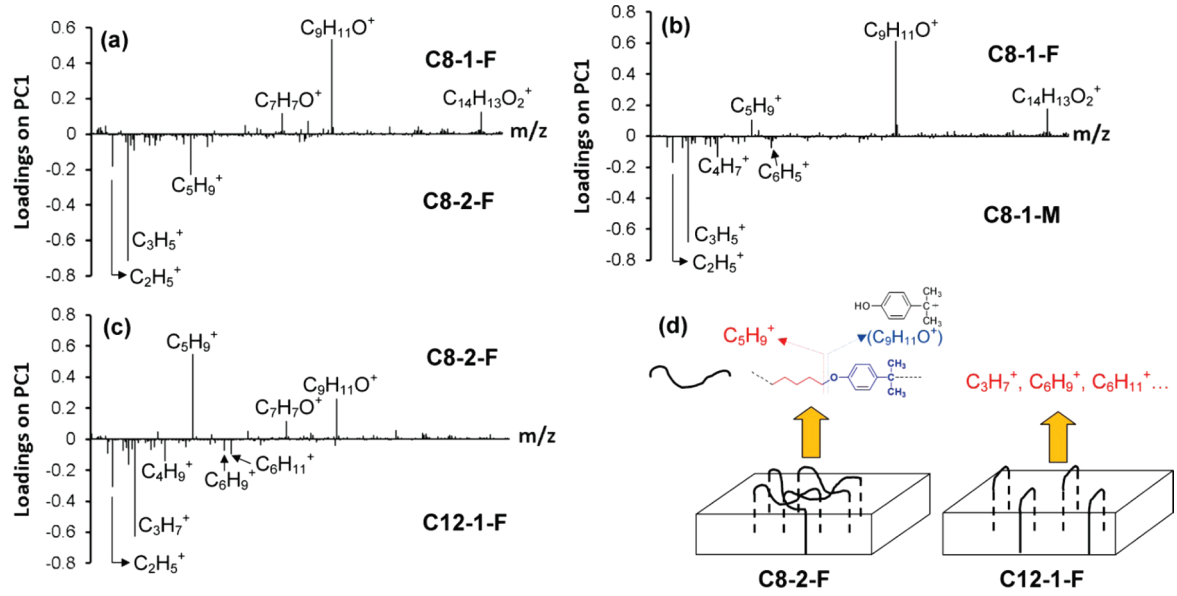

Figure 4. Standard loadings plots of positive ions, which compare between two selected groups of polymer surfaces: (a) C8-1-F vs C8-2-F, (b) C8-1-F vs C8-1-M, and (c) C8-2-F vs C12-1-F. (d) Proposed fold models for the groups of C8-2-F and C12-1-F, which are conducive to the ion fragmentation patterns shown on the positive and negative sign of the loadings.

number of CH_2 units, such as C12-1-F, has the most positive PC2 score, followed by those of the C10 polymers and then the C8 polymers. Obviously, it is much easier for a flexible chain than a rigid chain to overcome the torsional barrier and produce an ordered folding surface.

Both the PC1 and PC2 scores of the amorphous surfaces of the C*n* polymers tended to be more negative. These surfaces were mapped by the ions in group VI−X. The amorphous surface of the C12-1 polymer, C12-1-M, which is located in the PC1(−)−PC2(+) quadrant, is associated with the ions in group VI, while C10-1-M and C10-2-M are associated with the ions in groups VII and VIII, respectively. In addition, C8-1-M and C8-2-M are associated with the ions in group X and C8-3-M is associated with the ions in group IX. A common feature of the ions in these groups is that these ions normally have lower masses than the other groups of flexible- and rigid-segment ions that contribute to the folding surfaces of the C*n* polymers, such as those ions in groups I−V and group XI. This outcome points to the fact that the folding surfaces contain many impinged molecular folds and have a lower degree of structural disorder than the amorphous surfaces. Thereby, the folding surfaces lead to a higher probability of fragmentation of high-mass or even intact molecular ions. Figure 3d shows a schematic of the projection of the surface structures of the C*n* polymers onto the space of PC1 vs PC2. The schematic summarizes the previous interpretations of the PC scores (cf., Figure 3a) and the corresponding ion loadings (cf., Figure 3b,c). The two arrows indicate the effects of the increase of flexible-segment length and of the increase of the molecular weight on the surfaces. These are the two parameters that control the nature of SIMS ions.

To determine the changes in the structure of the folds as a function of molecular weight, we compare the composition between the folding surfaces of two selected C8 polymers using the standard loadings plots as shown in Figure 4a. In addition, the compositional changes of the polymer surface before and after crystallization are displayed in Figure 4b. As shown in Figure 4a, $C_9H_{11}O^+$ and $C_{14}H_{13}O_2^+$, which are typical rigid-segment ions of groups II and III, respectively (cf., Table 2), are distinctively associated with C8-1-F, while flexible-segment ions, such as $C_3H_5^+$ and $C_5H_9^+$, are associated with the surface of the higher-molecular weight polymer, C8-2-F. This suggests that C8-1-F contained relatively more rigid segment folds than C8-2-F and that as the molecular weight increased, the number of loops that contain both flexible and rigid segments at the folding surfaces increased. Figure 4b discriminates the amorphous surfaces from the crystallized surfaces of the C8-1 polymer. The increase of the concentration of $C_3H_5^+$ (a group VIII ion) is apparently one of the indicators of the increase of the degree of structural disorder at the surface.

The effect of the flexible-segment length on the composition of the folding surfaces was also studied. Two polymers, C8-2 and C12-1, with similar molecular weights were selected and the structural difference at the folding surfaces is shown by the loadings result in Figure 4c. The ions, such as $C_5H_9^+$, $C_7H_7O^+$, and $C_9H_{11}O^+$, which have positive loadings on PC1, are attributed to C8-2-F. On the other hand, only flexible-segment ions, including $C_2H_5^+$, $C_3H_7^+$, $C_4H_9^+$, and $C_6H_{11}^+$, are attributed to C12-1-F. This result suggests that there was a higher concentration of flexible-segment folds on C12-1-F than on C8-2-F. It is important to note that the $C_5H_9^+$ ion, which is a flexible-segment molecular ion in group XI, was exclusively attributed to C8-2-F. With the combination of the results shown in parts a and c of Figure 4, it is reasonable to assume that short uncrystallized stems, which comprised of partial flexible and rigid segments, as proposed in Figure 4d, were present at the folding surface of the C8-2 polymer, thereby resulting in concurrent fragmentation of $C_5H_9^+$ and $C_9H_{11}O^+$ ions.

The degree of the chemical variation among these surfaces was determined using the intensity ratios between two representative ions, $R_{j/k}$, by the following equation:

$$R_{j/k} = \frac{I_j/I_k}{I_j(\mathrm{s})/I_k(\mathrm{s})} \quad (1)$$

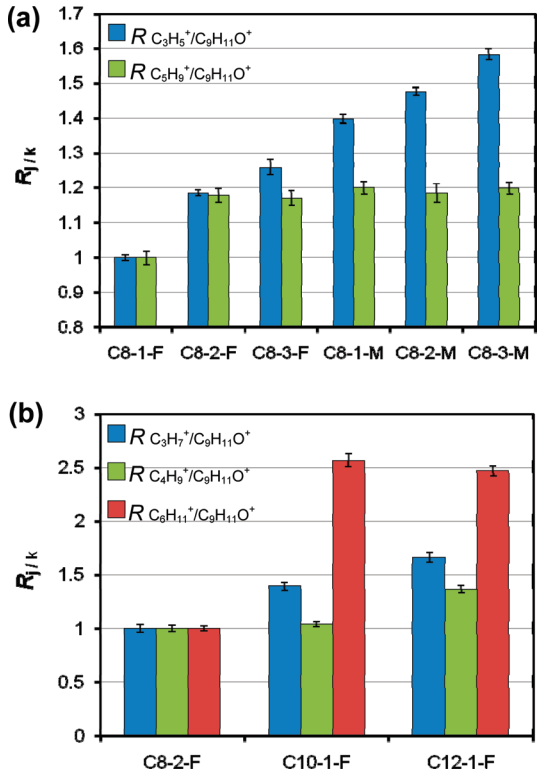

Figure 5. (a) $R_{j/k}$ values of a series of amorphous (M) and folding surfaces (F) of C8-1, C8-2, and C8-3 polymers with different molecular weights. (b) $R_{j/k}$ values of C8-2-F, C10-1-F, and C12-1-F.

where I_j and I_k represent the ion intensities of the positive ions, j and k, respectively. $I_j(s)/I_k(s)$ is the intensity ratio measured from a reference sample, s. We chose C8-1-F as the reference sample. Flexible-segment ions, $C_3H_5^+$ (in group VIII) and $C_5H_9^+$ (in group XI), which were shown to be associated with C8-3-M and C8-2-F, respectively, were chosen and their intensities were normalized against that of the rigid-segment ion, $C_9H_{11}O^+$, a group II ion, which contributed most to C8-1-F. Figure 5a shows the results for the amorphous and crystallized surfaces of the C8 polymers. The value of $R_{j/k}$ ($j = C_3H_5^+$ and $k = C_9H_{11}O^+$) increased by 1.4 times when the folding surface (C8-1-F) became amorphous (C8-1-M). When the same transition occurred between C8-2-M and C8-2-F and between C8-3-M and C8-3-F, the increase of $R_{j/k}$ became smaller (about 1.2). In addition, the value of $R_{j/k}$ ($j = C_5H_9^+$ and $k = C_9H_{11}O^+$) of the folding surfaces increased by1.2 times as the molecular weight of the C8 polymer increased from 9 000 (C8-1) to 16 000 g/mol (C8-3).

Figure 5b shows the intensity analyses, which provided further insights to distribution of the rigid and flexible segments on the folding surfaces of the C8, C10, and C12 polymers. C8-2-F was chosen as the reference sample (cf., eq 1). The intensities of three representative flexible-segment ions, $C_3H_7^+$, $C_4H_9^+$, and $C_6H_{11}^+$, were normalized against that of the rigid-segment ion, $C_9H_{11}O^+$. The value of $R_{j/k}$ was the largest with $j = C_6H_{11}^+$ even though all these ions, $C_3H_7^+$, $C_4H_9^+$, and $C_6H_{11}^+$, were strong outliers with negative PC1 loadings, as shown in Figure 4c. $C_4H_9^+$, which is located within the inner circle in the PC1(−)−PC2(+) quadrant, as shown in Figure 3c, has weaker connections with PC1 and PC2 than $C_3H_7^+$ and $C_6H_{11}^+$. This is a good example to illustrate the limitation of a standard loadings plot for variable selection although it is very convenient for a preliminary survey of the data structure by identification of the outliers in the plot. A correlation loadings plot can provide better information based on each variable's correlation and remove the unwanted effect of the size of the variables.

CONCLUSIONS

To conclude, in this article, we have provided a detailed interpretation of TOF-SIMS data for distinguishing the surface structures of the flat-on lamellae of a series of semiflexible C*n* polymers using PCA. The effects of the flexible-segment length and molecular weight of the polymers on the surface structure were studied. A 2-D projection of fold models onto the first two PC axes is proposed in accordance with the interpretation of the scores and loadings results of PCA based on positive ions. PC1 can be used to differentiate between rigid- and flexible-segment folds. PC2 can be used to determine the structural regularity of the folding surfaces. The proposed map of PC1 vs PC2 is aimed at predicting the fold chemical structures as a function of the molecular weight and the flexible-segment length of the C*n* polymers. The PCA results clearly show that the amount of flexible-segment folds increased against that of the rigid-segment folds when the flexible-segment length increased from 8 to 10 CH_2 units. An increase in the concentration of short loops of uncrystallized stems was observed on the folding surfaces when the molecular weight increased.

ACKNOWLEDGMENT

This work was funded by the Hong Kong Research Grants Council with the Grant Numbers 600405 and 600408.

SUPPORTING INFORMATION AVAILABLE

Additional information on the effects of autoscaling on the PCA of the same set of normalized intensities of positive ions (section A) and a brief discussion on the PCA of the negative ion spectra (section B). This material is available free of charge via the Internet at http://pubs.acs.org.

Received for review October 9, 2009. Accepted February 25, 2010.

AC902280H